Towards understanding kraft lignin depolymerisation under hydrothermal conditions

Original Article

Anders Ahlbom, Marco Maschietti, Rudi Nielsen, Merima Hasani* and Hans Theliander

Towards understanding kraft lignin depolymerisation under hydrothermal conditions

https://doi.org/10.1515/hf-2021-0121
Received June 28, 2021; accepted October 20, 2021;
published online November 15, 2021

Abstract: Kraft lignin depolymerisation using hydrothermal liquefaction suffers from the formation of char, resulting in a decreased product yield as well as causing operational problems. While this may be mitigated by the addition of capping agents such as phenol and isopropanol, other reaction parameters, for example reaction time and temperature, are also important for the product yields. In this work, the effect of short reaction times on the hydrothermal liquefaction of kraft lignin in an alkaline water and isopropanol mixture was investigated at 1–12 min and 290 °C. The results show that there were swift initial reactions: the major ether bonds in the lignin were broken within the first minute of reaction, and the molecular weight of all product fractions was halved at the very least. Longer reaction times, however, do not cause as pronounced structural changes as the initial reaction, indicating that a recalcitrant carbon-carbon skeleton remained in the products. Nevertheless, the yields of both char and monomers increased slowly with increasing reaction time. The swift initial depolymerising reactions were therefore followed by slower repolymerisation as well as a slow formation of monomers and dimers, which calls for careful tuning of the reaction time.

Keywords: HTL; hydrothermal liquefaction; isopropanol; kraft lignin.

***Corresponding author: Merima Hasani**, Department of Chemistry and Chemical Engineering, Chalmers University of Technology, SE-412 96 Gothenburg, Sweden, E-mail: merima.hasani@chalmers.se
Anders Ahlbom and Hans Theliander, Department of Chemistry and Chemical Engineering, Chalmers University of Technology, SE-412 96 Gothenburg, Sweden. https://orcid.org/0000-0002-5055-041X (A. Ahlbom)
Marco Maschietti and Rudi Nielsen, Department of Chemistry and Bioscience, Aalborg University, Niels Bohrs Vej 8, 6700 Esbjerg, Denmark

1 Introduction

Lignin has been acknowledged as a renewable source of aromatic compounds in the context of discovering alternatives to fossil resources. Such aromatic components have a downstream potential as precursors to chemicals and drop-in fuels (Ragauskas et al. 2006). Together with cellulose and hemicellulose, lignin constitutes the majority of lignocellulosic biomass which makes it appealing, since lignocellulosic biomass is widely available, renewable and does not compete directly with food production (Schutyser et al. 2018).

A heterogeneous polymer, lignin is mainly built up of three different types of monomers, namely *p*-coumaryl alcohol, coniferyl alcohol and sinapyl alcohol, where the frequency of each depends on the botanic origin of the lignin and the location in the plant. On extraction from biomass, however, the structure of lignin changes. For instance, the dominant chemical pulping process currently used, i.e. kraft pulping, breaks many of the inter-unit linkages, such as the β-O-4′ bonds, but also forms new carbon-carbon bonds leading to a more recalcitrant structure (Crestini et al. 2017; Gellerstedt 2015; Zakzeski et al. 2010). Nevertheless, the scale of the kraft pulping industry paired with techniques for extracting lignin from the cooking liquors, e.g. the LignoBoost process, makes it possible to recover large amounts of kraft lignin for subsequent use in material and chemical applications rather than simply incinerating it to recover energy which currently is the most common usage of the kraft lignin. A reasonably conservative estimate is that 6–9 million tons of kraft lignin could be extracted annually without significantly altering the energy balance of the mills involved (Berlin and Balakshin 2014). The availability of such large quantities makes discovering ways of valorising kraft lignin appealing in spite of its recalcitrance (Gellerstedt 2015). Such valorisation is commonly devised to begin with depolymerisation of the lignin, which provides aromatic components that can be upgraded later on to fuel additives and chemical precursors (Serrano et al. 2019; Vigneault et al. 2006).

Different depolymerisation approaches to liberate the aromatic units of lignin have been investigated, such as the use of oxidation, hydrogenolysis, pyrolysis and hydrothermal

methods (Evstigneyev and Shevchenko 2020; Schutyser et al. 2018). The latter method employs water at high temperature and pressure to depolymerise the lignin; the temperature can be used to control the main products of the process. Liquefaction is possible at intermediate temperatures, around 300–350 °C, yielding a liquid product from the lignin in a process denoted hydrothermal liquefaction (HTL); lower temperatures, around 200 °C, tend to favour solid formation while higher temperatures, around 600–700 °C, form gaseous products (Kruse and Dahmen 2015). In HTL the liquid product may be extracted with organic solvents to obtain an oil phase that is rich in monomers (Otromke et al. 2019). Alkaline conditions benefit the HTL process by increasing the oil yield and reducing the formation of char (Dunn and Hobson 2016). Such char formation is a general problem in the depolymerisation of lignin: a proportion of the lignin forms insolubles, as reactive components from the depolymerisation react with each other. To mitigate this problem, capping agents may be added to scavenge reactive fragments and thereby preventing them from forming char (Roberts et al. 2011). Other options are to shorten the reaction time and increase the heating rate (Bernhardt et al. 2021; Brand et al. 2014).

Several studies on various types of lignin, such as organosolv and acid hydrolysis lignin as well as lignosulphonates, in both continuous and batch reactors have shown that the oil and char yields are influenced by the reaction time (Cheng et al. 2012; Okuda et al. 2004; Roberts et al. 2011; Saisu et al. 2003; Yong and Matsumura 2012, 2013). In an early contribution on acid hydrolysis lignin Bobleter and Concin (1979) showed that a minimum of solid residue, 50 and 10%, could be obtained when the reaction time was limited to 3 and 0.4 min at 270 and 365 °C respectively, suggesting that the depolymerisation reactions were swift.

Subsequent studies on kraft lignin depolymerisation under hydrothermal conditions have not provided conclusive evidence of the effect of reaction time. Zhang et al. (2008) showed the char yield to reach a plateau within 6–15 min, the former at 374 °C and the latter at 300 °C. A similar result was obtained by Belkheiri (2018), who did not report any major changes to the char yield when reducing the reaction time from 11 to 6 min at 350 °C. However, even shorter reaction times alter the structure of kraft lignin, as shown by Abdelaziz et al. (2018), who demonstrated a reduction in the amount of large molecular weight components after only 2 min of reaction, even at temperatures below 250 °C. Abad-Fernández et al. (2019) showed kraft lignin to depolymerise within milliseconds when reacting in supercritical water. Moreover, Abad-Fernández et al. (2020) also showed that reaction times of mere seconds were sufficient to produce oil from kraft lignin at 300 °C. The depolymerisation of kraft lignin under HTL conditions thus appears to be a rapid process. Although previous research has illustrated that char levels reach a plateau, and that the content of large molecular weight compounds decreases during short reaction times, combined knowledge of the structural changes of solid fractions and the effects had by such changes on the yields under these conditions remains scarce.

In an earlier study the HTL of kraft lignin was investigated with respect to structural changes of the products and the resulting product yields (Ahlbom et al. 2021). In that study isopropanol was used as a capping agent and at a residence time of 12 min, isopropanol addition yielded lower amounts of char and a reduced molecular weight of the products. In the present work shorter reaction times were investigated, with focus on structural changes during the early phase of the reaction. Softwood kraft lignin was depolymerised in a small batch reactor, designed for swift heating with an injection system, at 250 bar and 290 °C, for 1–12 min using an alkaline water and isopropanol mixture as the reaction medium. The resulting reaction product was fractioned into three fractions and extensively characterised: molecular weight using gel permeation chromatography (GPC), changes in linkages and functional groups using nuclear magnetic resonance spectroscopy (NMR) and attenuated total reflectance Fourier transform infrared spectroscopy (ATR-FTIR) and, finally, the low-molecular weight compounds formed using gas chromatography mass spectrometry (GC-MS).

2 Materials and methods

2.1 Materials

LignoBoost lignin, a kraft lignin isolated from a mixture of *Picea abies* and *Pinus sylvestris* at the Bäckhammar Mill in Sweden, was used in all experiments. The dry content of the lignin was 78.8 ± 0.4 wt%, measured with a moisture analyser (Sartorius MA30; Sartorius, Göttingen, Germany). A mixture of isopropanol (VWR Chemicals, Fontenay-sous-Bois, France, >99.9%), anhydrous Na_2CO_3 (J.T. Baker, Deventer, The Netherlands, >99.5%) and deionised water was used as the reaction medium for the depolymerisation. Diethyl ether (DEE, Sigma-Aldrich, Steinheim, Germany, >99.0% with >1 ppm BHT as inhibitor), LiBr (Sigma-Aldrich, Steinheim, Germany, >99%), syringol (Aldrich, Steinheim, Germany, 99%), pullulan standards (Varian, Church Stretton, UK, PL2090-0100), DMSO (Dimethyl sulfoxide, Sigma-Aldrich, Steinheim, Germany, >99.7%), DMSO-d_6 (Sigma-Aldrich, Steinheim, Germany, 99.5 atom % D, 0.03% (*v/v*) TMS), HNO_3 (Merck Suprapur, Darmstadt, Germany, 65%) and sodium standard (UltraScientific, North Kingstown, USA) were used as received for analysis. 1 M HCl diluted inhouse was used for separation (Sharlau, Sentmenat, Spain, 37%).

2.2 Methods

LignoBoost kraft lignin was depolymerised at 290 °C, 250 bar and 1, 2, 4 and 12 min, respectively. The depolymerisation was performed in a

99 mL batch reactor (SITEC-Sieber Engineering AG, Zürich, Switzerland), in which all wetted parts were made of Inconel 625. This reactor was designed for an initial heating of a precharge containing no lignin, followed by an injection of a charge with lignin. The injection was charged at high pressure, with a precision hand pump, into the vapour-liquid equilibrium system prevailing in the preheated reactor. This allowed the lignin to be heated swiftly because the heat of condensation, released when the vapour of the precharge was condensed, heated the injection charge. An in-depth description of the reactor can be found elsewhere (Arturi et al. 2017).

The precharge used was a sodium carbonate solution that constituted around 60% by weight of the total feed to the reactor. After it was added to the reactor, nitrogen was used to displace air and it was sealed thereafter. The precharge was heated to 310 °C leading to a pressure of 98 bar, after which the injection charge, containing a sodium carbonate solution with isopropanol and lignin, was injected to reach a pressure of 165 bar. Since the injection aimed to reach a fixed pressure, rather than a specified amount of injected material, the composition of the reaction mixture varied somewhat, which can be seen in Table 1. A representative mixture of the precharge and injection charge had a pH of 10.1 ± 0.1 at ambient conditions.

The injection took approx. 40 s, during which time the temperature decreased to 240–260 °C, and then increased rapidly to 290 °C in the space of approx. 1 min after the end of the injection. This heating of the reaction medium raised the pressure towards the target of 250 bar, and the pressure was fine-tuned using the hand pumps to inject or eject <1 mL of injection charge. The high pressure meant that the reaction mixture was in an almost completely liquid state during the entire reaction. After the desired reaction time had passed, the reaction products were discharged swiftly into 200 mL of water placed in an ice water cold trap to quench the reaction.

The reaction time was defined as the time between the end of the injection and ejection of the material from the reactor. The average temperatures and pressures during the reaction, given in Table 1, were calculated using the formula $\Psi_{avg} = \int_{t_1}^{t_2} \Psi(t)dt/(t_2 - t_1)$ where t_2 was the time of discharge from the reactor, t_1 was the time when the injection was completed and Ψ was either the temperature or pressure. While all samples had the same nominal reaction temperature of 290 °C for the shorter reaction times, e.g. 1 and 2 min, the heating up of the reaction medium after injection formed a large part of the reaction time, resulting in the average temperature being below 290 °C. Furthermore, the increase in pressure also occurred in the early part of the reaction time, thus causing the average pressure of the sample at 1 min to be lower because the pressure was increasing for a larger fraction of the reaction time. Temperature and pressure profiles during the reaction are presented in Figure S1.

2.2.1 Product fractionation: The fractionation of the reaction product, outlined in Figure 1, produced three fractions: char, precipitated solids (PS), and acid soluble organics (ASO). The fractionation started with filtration of the diluted reaction product using filters having a nominal cut-off of 1.0–1.6 µm. Drying the resulting filter cake for 96 h in 40 °C gave the char fraction. The remaining filtrate was acidified with 1 M HCl to pH 1.5 (TitroLine 7000, SI Analytics; Xylem Analytics Germany GmbH, Welheim, Germany), which caused gas to be released, when the carbonates from the added Na_2CO_3 formed CO_2, and a brown material was precipitated. The acidified filtrate was centrifuged with a relative centrifugal force (RCF) at 3488×*g* for 5 min, after which a sample of the water phase was extracted with DEE to give a fraction to be investigated by GC-MS. The acidified filtrate was filtered once again, using filters with a nominal cut-off of 1.0–1.6 µm; the filter cake produced was dried for 120 h in 40 °C, giving the PS fraction. The filtrate of the acidified material was evaporated for 72 h in room temperature and for 24 h in 40 °C to yield the ASO fraction. The filtrate of the acidified material was also freeze dried (FreeZone Triad 7400030 freeze dryer; Labconco Corporation, Kansas City, MO, USA) for 96 h to remove as much water as possible for subsequent ATR-FTIR analysis.

2.2.2 Analytical procedures: Functional groups of the product fractions were investigated qualitatively with ATR-FTIR (PerkinElmer Frontier FT-IR; PerkinElmer Inc., Waltham, MA, USA). Absorbance was recorded over the spectrum 4000–400 cm^{-1}, with 4 cm^{-1} resolution and 10 scans per sample. Spectral processing, including standard baseline correction, was performed using PerkinElmer Spectrum (Vers. 10.4.3) and MATLAB R2020b.

The molecular weights of the product fractions were investigated using GPC (PL-GPC 50 Plus Integrated GPC system, Polymer Laboratories; Varian Inc., Church Stretton, UK). 10 mg of sample was dissolved in 1 mL of DMSO, with 10 mM LiBr. 0.1 mL of this solution was diluted with 4 mL of DMSO with 10 mM LiBr to a sample concentration of 0.24 mg/mL. The samples were filtered with a 0.2 µm syringe filter and run on a PL-GPC 50 Plus Integrated GPC system equipped with two PolarGel-M columns (300 × 7.5 mm) and one guard column (PolarGel-M (50 × 7.5 mm)). The flow rate was 0.5 mL/min and the temperature 50 °C. An ultraviolet light (UV) detector operating at 280 nm was employed and each sample was run in duplicate. Normalisation of the results was performed according to the equation $I_{i,n} = (I_i - I_{min})/(I_{max} - I_{min})$ where $I_{i,n}$ was the normalised intensity at point i, I_i the intensity at point i and I_{min} and I_{max} the minimum and maximum intensity of the measurement of the sample respectively. Samples were run in duplicates, with a relative standard deviation (RSD) of 0.43%. The data analysis was carried out using Cirrus GPC Software 3.2 and MATLAB R2019b.

Calibration of the GPC system was made with pullulan standards which are compatible with the system since they are soluble in DMSO. While being a common standard, pullulan is not ideal for lignin since the hydrodynamic volumes of the pullulan standards and lignin differ (Sulaeva et al. 2017). However, as remarked by Zinovyev et al. (2018), since it was the relative molecular weights between different fractions

Table 1: Average reaction temperatures and pressures, compositions, and product pH.

Reaction time (min)	T_{avg} (°C)	P_{avg} (bar)	Reaction product pH	Na_2CO_3 (wt%)	Water (wt%)	Isopropanol (wt%)	Lignin (dry) (wt%)
1	276	227	9.61	2.1	79.4	13.5	5.0
2	284	247	9.26	2.1	81.4	12.0	4.5
4	289	247	9.29	1.6	80.6	13.0	4.8
12	292	246	9.70	2.1	80.5	12.7	4.7

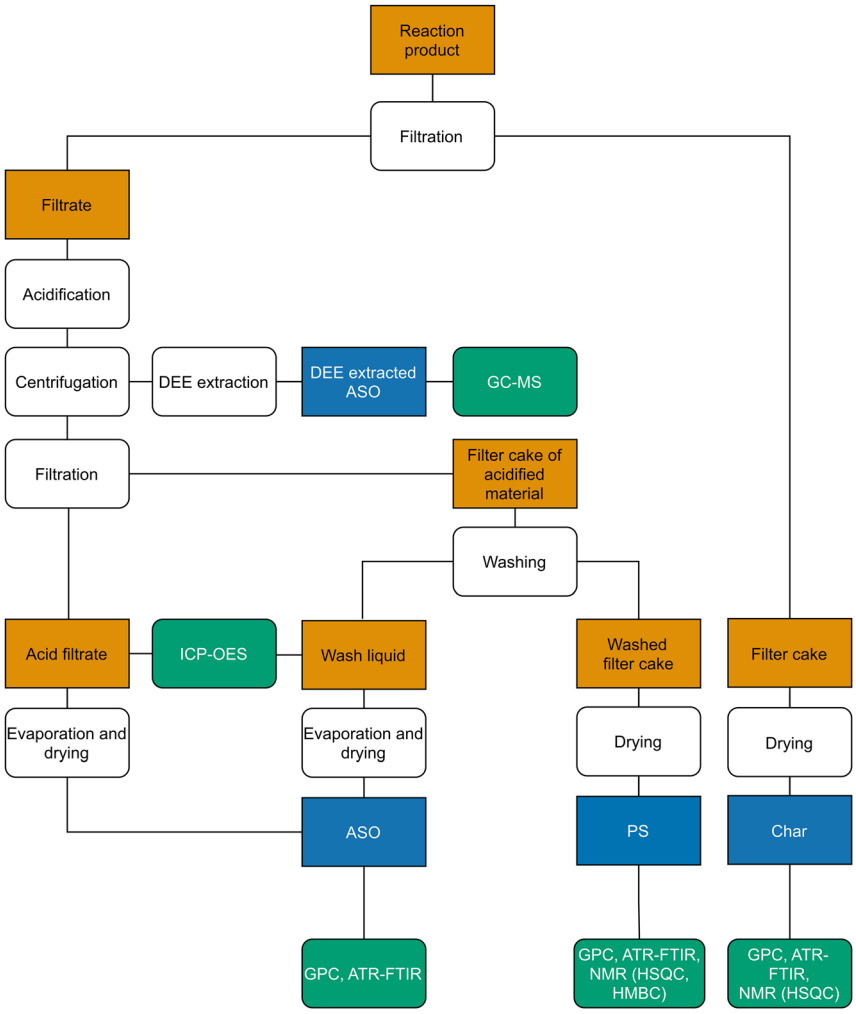

Figure 1: Flow chart of the fractionation of the HTL reaction product.

which were investigated in this work rather than exact molecular weights, pullulan standards were deemed acceptable.

GC-MS (Agilent 7890A; Agilent Technologies Co. Ltd., Shanghai, China, and Agilent 5975C; Agilent Technologies Inc., Wilmington, DE, USA) was used to investigate low-molecular weight components in the water phase. To 10 mL of the acidified phase, 1 mL of 0.001 g/mL syringol in water was added as an internal standard. Syringol was chosen because it has a similar structure to the products anticipated without being formed itself during the reaction, since the lignin was sourced from softwood. The mixture was extracted, 1:1 *w/w*, with DEE. 2 mL of the DEE phase filtered with a 0.45 µm syringe filter and run in the GC-MS. The injection temperature was 300 °C, the split ratio 19:1 and injection volume 1 µL. The heating programme began at 70 °C, which was held for 2 min; this was followed by heating at a rate of 20 °C/min up to 275 °C and held at this temperature for 10 min. Helium, the carrier gas, had a flow rate of 1 mL/min and the MS source was operated at 230 °C with the quadrupole at 150 °C. The NIST MS Search Programme (Vers. 2.2) was used for product identification using the library NIST/EPA/NIH Mass Spectral Library (NIST 11). A semi-quantification of the products identified with GC-MS was made as in the work of Nguyen et al. (2014) using the internal standard and the relationship: $W_i = W_{IST}A_i/A_{IST}$, where W was the mass fraction and A the area in the chromatogram, while *IST* denoted the internal standard and *i* the species, respectively. The samples were run in single, with selected test samples repeated in triplicate, giving an RSD of 8.1%.

2D NMR analyses were used to examine the structure of the LignoBoost lignin, char and PS, thus tracking the structural changes during the reaction (Balakshin et al. 2021). Both the heteronuclear single quantum coherence (HSQC) and heteronuclear multiple bond correlation (HMBC) pulse sequences were used, the latter to investigate the presence of carbonyl compounds. The samples were prepared by dissolving 35 mg of sample in 0.25 ml of DMSO-d_6. They were then centrifuged in Eppendorf tubes with an RCF at 20,879×*g* for 5 min, and the supernatant was transferred with a syringe to 3 mm tubes. A small amount of the char and LignoBoost lignin, less than 5% by weight, remained undissolved and accordingly was not included in the analysis. The PS fraction, on the other hand, did not display any undissolved material.

HSQC spectra were recorded at 25 °C on a 700 MHz spectrometer with a 5 mm QCl cold probe (Bruker Avance III; Bruker BioSpin GmbH, Rheinstetten, Germany) and an 800 MHz spectrometer using a 5 mm TXO cold probe (Bruker Avance III HD; Bruker BioSpin GmbH, Rheinstetten, Germany). The pulse programme used was *hsqcedetgpsisp2.3* with 91 ms acquisition time for ^{1}H and 8 ms for ^{13}C, an FID size of 2560 and 256 points, respectively, and 32 scans, with 1 s relaxation delay, on the 700 MHz spectrometer. The char sample of 1 min of reaction was recorded with 64 scans for reasons of sensitivity. The

same pulse programme was used on the 800 MHz spectrometer with acquisition times of 79 ms for ^{1}H and 6 ms for ^{13}C, an FID size of 2560 and 512 points, respectively, and 24 scans with 1 s relaxation delay. The HSQC spectra were recorded in an edited fashion.

HMBC spectra were recorded at 25 °C using the pulse programme *hmbcetgpl3nd* on the 700 MHz spectrometer. An acquisition time of 291 ms was used for ^{1}H and 7 ms for ^{13}C, the size of the FID was 8192 and 512, respectively, optimized for long range J_{HC} couplings of 8 Hz, with 40 scans and a 1.5 s relaxation delay. HMBC experiments were also recorded on the 800 MHz spectrometer with parameters equivalent to the 700 MHz spectrometer with the exception that the acquisition time was 254 ms for ^{1}H and 6 ms for ^{13}C. Processing of all NMR spectra was carried out with MestReNova (Vers. 10.0.2) and calibration of the chemical shifts was done with the central solvent peak. i.e. DMSO-d_6 at 2.50 and 40.20 ppm.

The salt content of the acid filtrate and acid wash liquid (cf. Figure 1) was estimated by measuring the sodium content of the liquids with inductively-coupled plasma optical emission spectroscopy (ICP-OES, Thermo Scientific iCAP 6500; Thermo Fischer, Cambridge, UK), at 818 nm. The liquids were diluted at a ratio of 1:20 with 0.5 M HNO_3 and run in triplicate in the ICP-OES. The average RSD was found to be 13% for all samples: 3% for the acid filtrate and 23% for the acid wash liquid. This salt content was deducted from the ASO.

3 Results and discussion

The reaction product was an aqueous suspension with no visible hydrophobic oily phase. The suspension had a distinct smoky smell and was brown in colour. The fractionation yielded the char and PS from the aqueous phase as dark brown powders, and the ASO as orange-brown films on the walls of the drying containers.

3.1 Molecular weights

The GPC chromatograms for the char (A), PS (B) and ASO (C) are presented in Figure 2 together with the original lignin. The molecular weight distribution of the char and PS for all reaction times was narrow compared to the original lignin used; the biggest change was due to the largest molecular weight fractions decomposing, similar to the findings of Abdelaziz et al. (2018). However, both the char and PS retained fractions with a relatively high molecular weight: the peak positions were around 7000 Da. The ASO, on the other hand, displayed a wholly different distribution compared to the char and PS, with a much larger fraction of low molecular weight compounds. The large peak around 2000 Da, however, meant the ASO were not only comprised of monomers and dimers, but also larger molecules that remained soluble in the acid solution.

The weight average molecular weights (M_w) of the product fractions are reported in Table 2. It was notable that, compared to the original lignin, the M_w of char and PS was

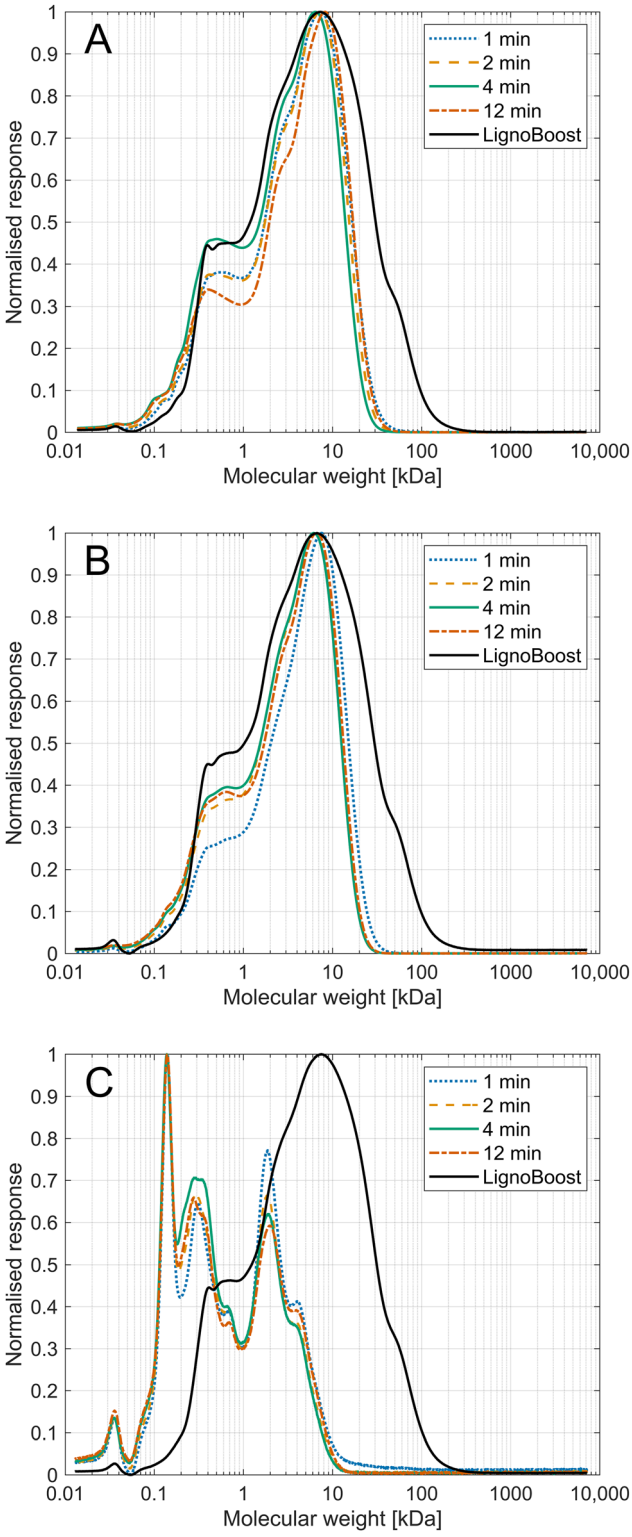

Figure 2: GPC chromatograms for char (A), PS (B) and ASO (C).

halved after only 1 min of reaction. The temperature of the reaction mixture was still rising during this short reaction time and yet the lignin reacted. An even lower reaction temperature may thus be feasible whilst the lignin is being

depolymerised. Large molecular weight products remained in all fractions, however, despite the swift initial reaction.

With increasing reaction time, the molecular weight continued to decrease for all fractions until a minimum was reached, which was observed after 4 min of reaction. At 12 min of reaction, a slight increase in the molecular weight could be observed, being most notable for the char fraction. Although the initial depolymerisation process was very swift, repolymerisation was thus a slower process that started to exceed the rate of depolymerisation later on during the reaction, which agreed with the two-step reaction model of Zhang et al. (2008). The combined effect of depolymerisation and repolymerisation resulted in a net increase of the molecular weight between 4 and 12 min of reaction.

3.2 Structural changes

The major inter-unit linkages of lignin can be traced via peaks in the inter-unit aliphatic region of the HSQC spectra: δ_C/δ_H 52–90/2.8–5.7 ppm (Crestini et al. 2017; Mattsson et al. 2016). Examples of such linkages are the β-O-4′, β-β′ and β-5′ bonds (Mattsson et al. 2016). It is the connection with oxygen that shifts the carbon signals to this region: the C_α ether linkages of β-β′ (pinoresinol) and β-5′ are visible in this part of the spectrum, even though their carbon-carbon bonds are not.

The inter-unit aliphatic regions of the LignoBoost lignin, char and PS after 1 min of reaction are presented in Figure 3, with the positions of the inter-unit linkages marked with black rectangles. The major inter-unit lignin linkages disappeared as soon as after 1 min of reaction, as their C–O bonds break. The signal for methoxy groups on the aromatic rings, however, remained strong at 56 ppm: such methoxy ether bonds thus remained while the inter-unit ether linkages were cleaved. In addition, there were some signals that remained in the inter-unit aliphatic region, such as those for the β-β′ bond at δ_C/δ_H 86/4.65 ppm, in the PS spectrum (Figure 3C). However, along with other signals remaining in the black rectangles in the char (Figure 3B) and PS (Figure 3C) spectra, these signals disappeared at longer reaction times (cf. Figure S2). Abdelaziz et al. (2018) also noted that the inter-unit linkages in their oil fraction disappeared after 2 min of reaction at 240 °C when using the HSQC pulse sequence, but did not investigate fractions resembling either the char or the PS with HSQC.

Table 2: Weight average molecular weight (M_w) of the product fractions and lignin, with respective standard deviation.

Reaction time (min)	Char (kDa)	PS (kDa)	ASO (kDa)	Lignin (kDa)
1	5.88 ± 0.01	5.85 ± 0.01	1.68 ± 0.02	12.2 ± 0.4
2	5.42 ± 0.01	4.58 ± 0.00	1.30 ± 0.02	
4	4.69 ± 0.00	4.47 ± 0.01	1.18 ± 0.01	
12	6.05 ± 0.00	4.71 ± 0.00	1.32 ± 0.01	

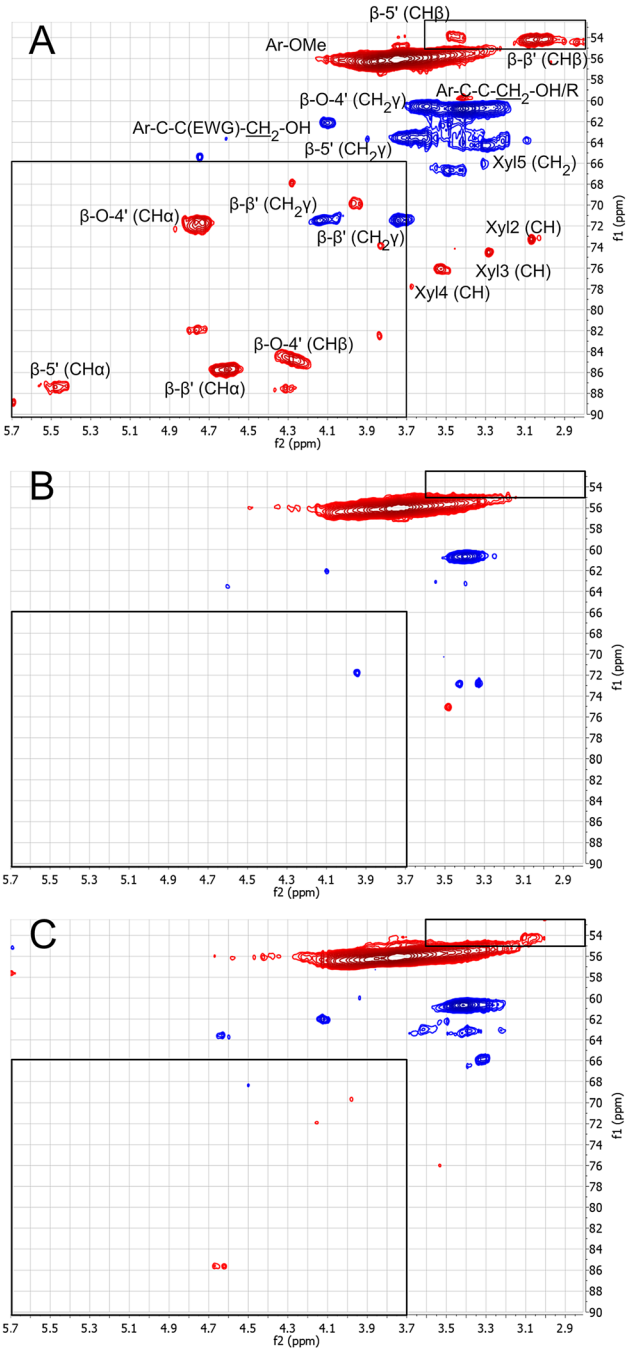

Figure 3: Inter-unit aliphatic region of the HSQC spectra of unreacted LignoBoost lignin (A), char (B) and PS (C) after 1 min of reaction time. Annotations in the LignoBoost spectrum (A) are made according to Crestini et al. (2017) and Mattsson et al. (2016). The specifications within the parentheses in (A) denote to which C–H coupling the annotation belongs. EWG: electron-withdrawing group and Xyl: xylan.

NMR measurements thus confirmed the GPC results of a swift reaction and show that the product fractions were not just unreacted lignin, yet the content of high molecular weight products in all fractions shown by GPC measurements suggests that recalcitrant bonds remained. Mattsson et al. (2016) also noted that the carbon-carbon skeleton of the β-β′ and β-5′ bonds might remain even though their C–O bonds were broken during HTL.

While both the char and PS fraction displayed similar results in the inter-unit aliphatic region, the aliphatic region of the spectra δ_C/δ_H 10–55/0–3 ppm, showed larger differences between the product fractions, as shown in Figure 4. The char fraction had markedly fewer peaks in this region (Figure 4B) compared to the starting lignin (Figure 4A) and the PS (Figure 4C), indicating a smaller amount of aliphatic side chains in the char. The PS, on the other hand, retained most of the aliphatic bonds from the lignin (Figure 4C).

3.3 Functional groups

Additional analyses of the quaternary and carbonyl carbon atoms, which the HSQC pulse programme is unable to detect due to their lack of a C–H bond, were made using the HMBC pulse programme on the PS fraction that had reacted for 4 min, the results of which are presented in Figure 5. The HMBC sequence show multiple bond correlations, for instance H and C atoms which are separated by two, three or even more bonds which enables detection of cross peaks with carbonyl carbons and protons at a multiple bond distance (McClelland et al. 2017). Thus, carbonyl carbons without a C–H bond can be investigated. No signal could be detected in the HMBC investigation of the char fraction, possibly due to agglomerates of char quenching the signal.

The results obtained for both the LignoBoost lignin and the PS (Figures 5A and 5B respectively) showed signals of carbon atoms with high shifts typical of carbonyl groups. These carbonyl groups, marked with black rectangles in the figures, are annotated as carboxylic acids and esters by McClelland et al. (2017).

Likely, the carbonyl groups of the PS were connected to aliphatic units, since cross peaks between carbonyl groups and aliphatic protons were present in the black rectangles of the HMBC spectra (Figure 5). No cross peaks between carbonyl carbons and aromatic protons, which would appear around 165–185/6–8 ppm, were seen in the HMBC spectra indicating that the carbonyl groups were not attached to the aromatic ring. Moreover, studies by González et al. (2004) on the lignin model compound vanillic acid show that carboxylic groups on the aromatic ring become rapidly decarboxylated under hydrothermal conditions.

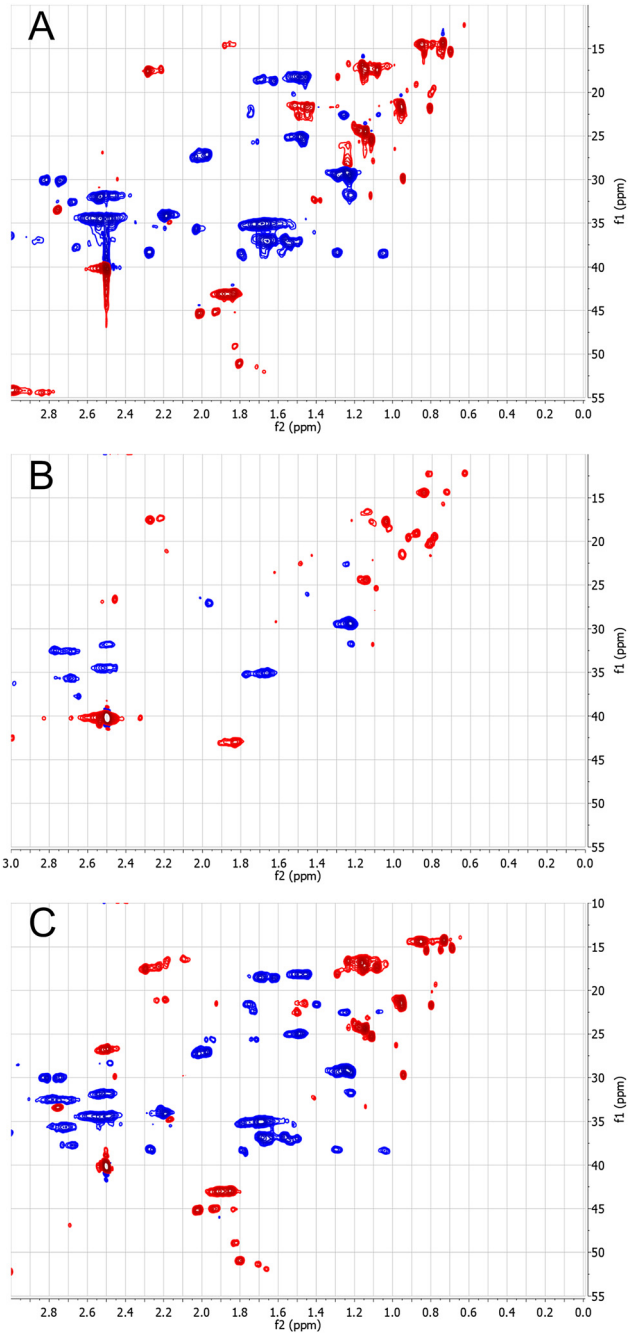

Figure 4: Aliphatic region of the HSQC spectra of LignoBoost lignin (A), char (B) and PS (C) after 1 min of reaction time.

ATR analyses of the product fractions confirmed that carbonylic moieties were present in the ASO and PS via a clear signal at 1700 cm^{-1}, as shown in Figures 6 and S3, respectively. The ATR results for the PS thus supported the conclusion drawn from the HMBC experiments that carboxylic acids or esters were present. This agreed with the precipitation of the solids at lower pH as the acid functionalities were protonated.

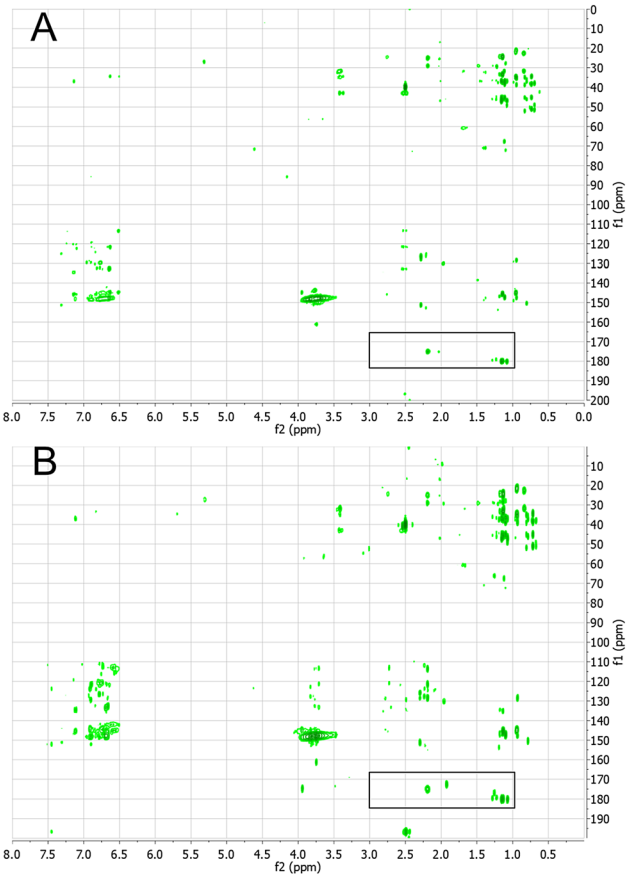

Figure 5: HMBC spectra of unreacted LignoBoost lignin (A) and PS (B) after 4 min of reaction. Peaks within the black rectangles correspond to carbonyl groups.

Along with the polar carbonyl groups, the ASO also display hydroxyl groups (Figure 6), which resonate at 3042–3695 cm^{-1} (Faix 1992). Probably, these polar groups kept the ASO solubilised in the acidified reaction product despite their high molecular weight.

No carbonyl signal at 1700 cm^{-1} was visible in the spectra of the char samples (Figure 7) and the hydroxyl group region, 3042–3695 cm^{-1}, was less pronounced than in the ASO fractions. This lack of polar moieties agreed with the char being insoluble in the polar reaction liquid. Notably, the polar groups kept the PS fraction dissolved after the reaction whereas the char precipitated, despite the two fractions having a similar M_w (Table 2).

While clear changes could be seen in all the ATR spectra of the product fractions when compared to the original lignin spectrum (Figures 6 and 7 and Figure S3), none of the fractions showed any major differences between the various reaction times. The functional groups detectable by ATR-FTIR in all the fractions thus appeared to change only slightly during the reaction time, once the swift initial reaction phase that degraded the original kraft lignin structure had passed. This concurred with the molecular weights changing only a little after 1 min of reaction.

3.4 Yields

The yields of the isolated fractions versus the dry lignin feed are presented in Figure 8. Full mass balance closure

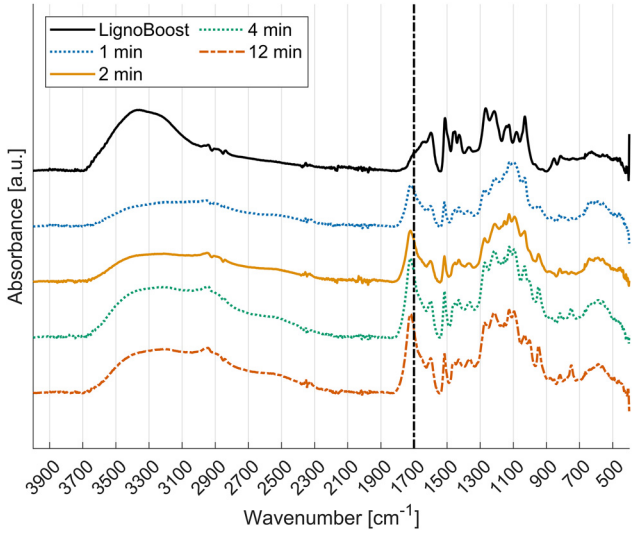

Figure 6: ATR spectra of the ASO, with the 1700 cm^{-1} carbonylic wave number marked by the dashed black line.

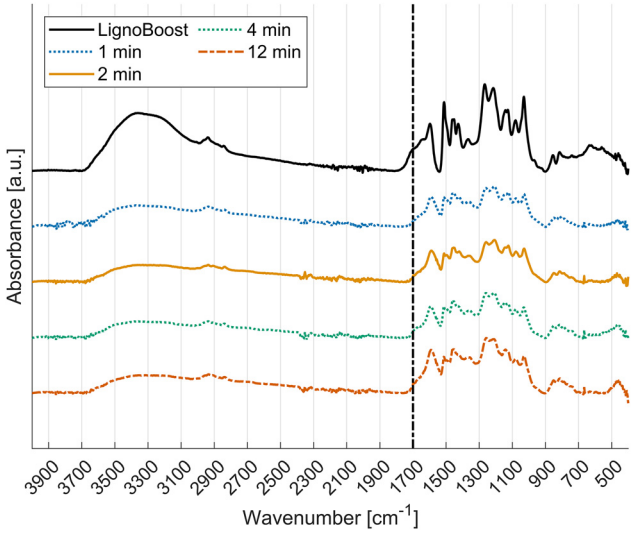

Figure 7: ATR spectra of the char. N.B. No 1700 cm^{-1} peak can be seen (black dashed line).

was not attained, in agreement with other batch reactor studies, e.g. by Ye et al. (2012) and Lee et al. (2016). Longer reaction times led to more char being formed, which was an expected result, due to repolymerisation reactions. The yield of the PS, on the other hand, decreased with increasing reaction time and might be interpreted as the PS reacting and forming char at longer reaction times. At 12 min of reaction time, the results could be compared to results of Ahlbom et al. (2021), with very similar yield results for both char and PS, although the yield of ASO was halved in the present study.

Provided that the aliphatic side chains carried many of the functional units that solubilised the PS before acidification, such as carboxylic acids and hydroxyl groups, cleavage of these side chains from the aromatic ring would cause the PS to form char. PS could therefore form char at longer reaction times as they were losing their side chains: this is most likely what is observed in Figure 8, where the yield of PS decreased whilst that of char increased. The alkyl side chains may in turn end up in the ASO phase owing to their content of functional groups keeping them solubilised.

The PS fraction indeed showed peaks that were greater in both number and intensity in the aliphatic region of the HSQC spectra compared to the char, which would indicate a lower amount of aliphatic side chains in the char fraction (Figure 4). This agreed with the char precipitating due to a lack of aliphatic side chains with functional groups on them.

3.5 Low molecular weight compounds

The compounds identified with GC-MS were phenolic and, at longer reaction times, their yields increase as shown in Table 3. These yields were in agreement with results reported in other HTL studies with kraft lignin at 280–300 °C (Arturi et al. 2017; Beauchet et al. 2012). Although the method of quantifying samples with GC-MS was semiquantitative, the trends were consistent: the yield of each identifiable compound increased with reaction time, as shown in Figure 9. The increased yield of monomers at longer reaction times could be potentially explained by the later cleavage of carbon-carbon bonds, which caused monomers to form.

The high yield of 2-methoxyphenol, i.e. guaiacol, relative to the other compounds agreed with the original lignin being sourced from softwood. Notably, the yield of 2-methoxyphenol increased over the entire time range: it is typically reported to decrease with increasing reaction time since it decomposes into, for instance, catechol (Beauchet et al. 2012; Belkheiri 2018; Rößiger et al. 2017). Increasing the temperature has also been reported to decrease the yield of 2-methoxyphenol (Arturi et al. 2017). At the temperatures used in this study, however, the decomposition rate of 2-methoxyphenol did not overcome the formation rate within the reaction time. It was nonetheless possible that a reaction time longer than 12 min at 290 °C could reduce the yield of guaiacol.

Table 3: Total yield of components identified with GC-MS.

Reaction time (min)	Total yield of components identified with GC-MS versus dry lignin (%)
1	2.2
2	3.1
4	4.1
12	4.8

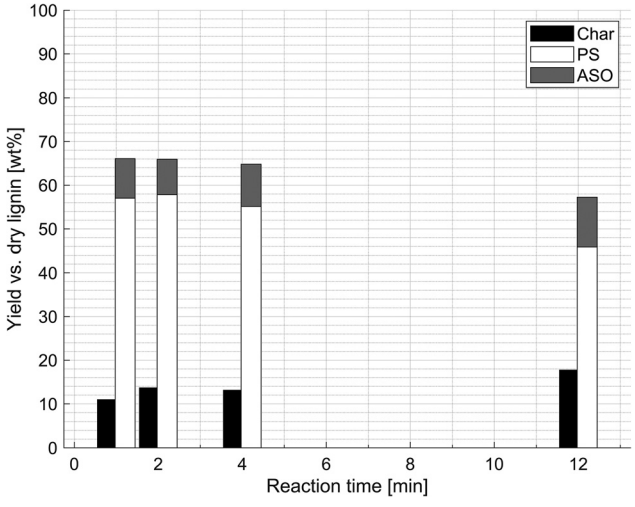

Figure 8: Yield of product fractions versus reaction times.

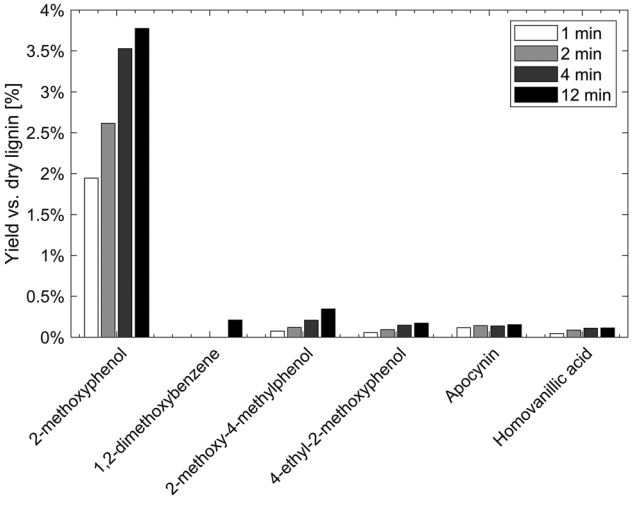

Figure 9: The most prevalent compounds (as identified with GC-MS) and their yields versus lignin.

The alkyl guaiacols identified, namely 4-ethyl-2-methoxy phenol and 2-methoxy-4-methyl phenol, were both substituted on the fourth position. This suggests that they originated from a shortened side chain, indicating that side chains were cleaved during the reaction (Ehara et al. 2005).

3.6 Tentative reaction progression

HTL of kraft lignin quickly broke inter-unit ether linkages as seen in the HSQC spectra in Figure 3. The carbon-carbon bonds are more stable than the inter-unit C–O bonds (Parthasarathi et al. 2011; Roberts et al. 2011; Shuai et al. 2016), and while the latter broke quickly under these conditions the carbon-carbon bonds may thus remain. The process of cleaving side chains from the structures as well as cleaving other carbon-carbon bonds was likely slower than the initial C–O breakage, which explains why a high molecular weight was retained after the initial reaction for the char and PS (Table 2). The retained high molecular weight also indicated that inter-unit C–O bonds were not as prevalent as carbon-carbon bonds since a large molecular weight network was retained after the inter-unit C–O cleavage. In addition, kraft pulping broke a large fraction of the ether linkages of lignin, which meant the kraft lignin already at the outset had a reduced content of C–O bonds.

With increased reaction times, more carbon-carbon bonds could be cleaved, reducing the M_w, and yielding more low molecular weight compounds. However, repolymerisation reactions occurred at longer reaction times, as evidenced by the higher M_w at 12 min of reaction (Table 2), as well as the increased yield of char. Char yields could also increase by PS losing alkyl side chains bearing polar groups. Those PS fragments could thus precipitate as char while the alkyl side chains may end up in the ASO fraction due to their content of polar groups. In Figure 10 a tentative overview of the reaction over time is outlined.

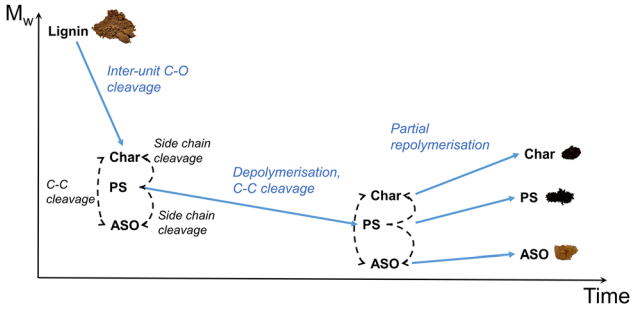

Figure 10: Tentative reaction diagram illustrating the evolution of molecular weights during the reaction as well as figures of the fractions and starting material.

4 Conclusions

Kraft lignin depolymerisation at hydrothermal conditions (290 °C and 250 bar, with isopropanol and Na_2CO_3) appeared to be a swift process. Rearrangement of the lignin structure and partial depolymerisation of the lignin occurred already after 1 min of reaction, as evidenced by a reduced molecular weight, shown by GPC measurements, and the breaking of major inter-unit linkages, as shown by NMR analyses. The swiftness of the reaction was also revealed in the ATR-FTIR results: the functional groups of the products showed little change after the rapid reactions that occur during the first minute of reaction. The persistence of high molecular weight fractions indicated, however, that recalcitrant carbon-carbon bonds were present in the products.

The yield of solids precipitated at pH 1.5, the precipitated solids, was the major product, but the yield decreased with increasing reaction time. On the other hand, with increasing reaction time, the yield of char increased, cleavage of side chains of precipitated solids could possibly explain this. Moreover, the rate of repolymerisation reactions began to exceed the rate of further depolymerisation between 4 and 12 min of reaction, which also increased the char yield. Finally, GC-MS analyses indicated that the yield of monomeric phenolic structures increased with increasing reaction time.

Abbreviations

ASO	Acid Soluble Organics
ATR	Attenuated Total Reflectance
BHT	Butylated Hydroxytoluene
DEE	Diethyl Ether
DMSO	Dimethyl Sulfoxide
DMSO-d_6	Deuterated Dimethyl Sulfoxide
EWG	Electron Withdrawing Group
FID	Free Induction Decay
FTIR	Fourier Transform Infrared Spectroscopy
GC	Gas Chromatography
GPC	Gel Permeation Chromatography
HMBC	Heteronuclear Multiple Bond Correlation
HSQC	Heteronuclear Single Quantum Coherence
HTL	Hydrothermal Liquefaction
ICP-OES	Inductively-Coupled Plasma - Optical Emission Spectrometry
MS	Mass Spectrometry
M_w	Weight Average Molecular Weight
NMR	Nuclear Magnetic Resonance
PS	Precipitated Solids
RCF	Relative Centrifugal Force
RSD	Relative Standard Deviation
UV	Ultraviolet light
Xyl	Xylan

Acknowledgements: The thanks of the authors go to Ms. Dorte Spangsmark for her analytical contributions to the experiments, Dr. Stellan Holgersson for his technical support with the ICP-OES measurements, Dr. Ulrika Brath for her technical support with the NMR analysis at the Swedish NMR Centre at the University of Gothenburg and Ms. Maureen Sondell for her language review of the manuscript.
Author contributions: All the authors have accepted responsibility for the entire content of this submitted manuscript and approved submission.
Research funding: This work was funded by the Swedish Energy Agency, which had no other involvement in the study.
Conflict of interest statement: The authors declare no conflicts of interest regarding this article.

References

Abad-Fernández, N., Pérez, E., and Cocero, M.J. (2019). Aromatics from lignin through ultrafast reactions in water. Green Chem. 21: 1351–1360.

Abad-Fernández, N., Pérez, E., Martín, Á., and Cocero, M.J. (2020). Kraft lignin depolymerisation in sub- and supercritical water using ultrafast continuous reactors. Optimization and reaction kinetics. J. Supercrit. Fluids 165: 104940.

Abdelaziz, O.Y., Li, K., Tunå, P., and Hulteberg, C.P. (2018). Continuous catalytic depolymerisation and conversion of industrial kraft lignin into low-molecular-weight aromatics. Biomass Convers. Biorefinery 8: 455–470.

Ahlbom, A., Maschietti, M., Nielsen, R., Lyckeskog, H., Hasani, M., and Theliander, H. (2021). Using isopropanol as a capping agent in the hydrothermal liquefaction of kraft lignin in near-critical water. Energies 14: 932.

Arturi, K.R., Strandgaard, M., Nielsen, R.P., Søgaard, E.G., and Maschietti, M. (2017). Hydrothermal liquefaction of lignin in near-critical water in a new batch reactor: influence of phenol and temperature. J. Supercrit. Fluids 123: 28–39.

Balakshin, M.Y., Capanema, E.A., Sulaeva, I., Schlee, P., Huang, Z., Feng, M., Borghei, M., Rojas, O.J., Potthast, A., and Rosenau, T. (2021). New opportunities in the valorization of technical lignins. ChemSusChem 14: 1016–1036.

Beauchet, R., Monteil-Rivera, F., and Lavoie, J.M. (2012). Conversion of lignin to aromatic-based chemicals (L-chems) and biofuels (L-fuels). Bioresour. Technol. 121: 328–334.

Belkheiri, T. (2018). *Hydrothermal liquefaction of lignin in sub-critical water to produce biofuel and chemicals*, Ph.D. thesis. Gothenburg, Chalmers University of Technology.

Berlin, A. and Balakshin, M. (2014). Industrial lignins: analysis, properties, and applications. In: Gupta, V.K., Tuohy, M.G., Kubicek, C.P., Saddler, J., and Xu, F. (Eds.), *Bioenergy research: advances and applications*. Elsevier, Amsterdam, pp. 315–336.

Bernhardt, J.J., Rößiger, B., Hahn, T., and Pufky-Heinrich, D. (2021). Kinetic modeling of the continuous hydrothermal base catalyzed depolymerization of pine wood based kraft lignin in pilot scale. Ind. Crop. Prod. 159: 113119.

Bobleter, O. and Concin, R. (1979). Degradation of poplar lignin by hydrothermal treatment. Cellul. Chem. Technol. 13: 583–593.

Brand, S., Hardi, F., Kim, J., and Suh, D.J. (2014). Effect of heating rate on biomass liquefaction: differences between subcritical water and supercritical ethanol. Energy 68: 420–427.

Cheng, S., Wilks, C., Yuan, Z., Leitch, M., and Xu, C. (2012). Hydrothermal degradation of alkali lignin to bio-phenolic compounds in sub/supercritical ethanol and water-ethanol co-solvent. Polym. Degrad. Stabil. 97: 839–848.

Crestini, C., Lange, H., Sette, M., and Argyropoulos, D.S. (2017). On the structure of softwood kraft lignin. Green Chem. 19: 4104–4121.

Dunn, K.G. and Hobson, P.A. (2016). Hydrothermal liquefaction of lignin. In: O'Hara, I. and Mundree, S. (Eds.), *Sugarcane-based biofuels and bioproducts*. John Wiley & Sons, Inc., Hoboken, New Jersey, pp. 165–206.

Ehara, K., Takada, D., and Saka, S. (2005). GC-MS and IR spectroscopic analyses of the lignin-derived products from softwood and hardwood treated in supercritical water. J. Wood Sci. 51: 256–261.

Evstigneyev, E.I. and Shevchenko, S.M. (2020). Lignin valorization and cleavage of arylether bonds in chemical processing of wood: a mini-review. Wood Sci. Technol. 54: 787–820.

Faix, O. (1992). Fourier transform infrared spectroscopy. In: Lin, S.Y. and Dence, C.W. (Eds.), *Methods in lignin chemistry*. Springer Science & Business Media, Berlin, pp. 83–109.

Gellerstedt, G. (2015). Softwood kraft lignin: raw material for the future. Ind. Crop. Prod. 77: 845–854.

González, G., Salvadó, J., and Montané, D. (2004). Reactions of vanillic acid in sub- and supercritical water. J. Supercrit. Fluids 31: 57–66.

Kruse, A. and Dahmen, N. (2015). Water – a magic solvent for biomass conversion. J. Supercrit. Fluids 96: 36–45.

Lee, H.-S., Jae, J., Ha, J.-M., and Suh, D.J. (2016). Hydro- and solvothermolysis of kraft lignin for maximizing production of monomeric aromatic chemicals. Bioresour. Technol. 203: 142–149.

Mattsson, C., Andersson, S.I., Belkheiri, T., Åmand, L.E., Olausson, L., Vamling, L., and Theliander, H. (2016). Using 2D NMR to characterize the structure of the low and high molecular weight fractions of bio-oil obtained from LignoBoost™ kraft lignin depolymerized in subcritical water. Biomass Bioenergy 95: 364–377.

McClelland, D.J., Motagamwala, A.H., Li, Y., Rover, M.R., Wittrig, A.M., Wu, C., Buchanan, J.S., Brown, R.C., Ralph, J., Dumesic, J.A., et al. (2017). Functionality and molecular weight distribution of red oak lignin before and after pyrolysis and hydrogenation. Green Chem. 19: 1378–1389.

Nguyen, T.D.H., Maschietti, M., Belkheiri, T., Åmand, L.E., Theliander, H., Vamling, L., Olausson, L., and Andersson, S.I. (2014). Catalytic depolymerisation and conversion of kraft lignin into liquid products using near-critical water. J. Supercrit. Fluids 86: 67–75.

Okuda, K., Umetsu, M., Takami, S., and Adschiri, T. (2004). Disassembly of lignin and chemical recovery – rapid depolymerization of lignin without char formation in water-phenol mixtures. Fuel Process. Technol. 85: 803–813.

Otromke, M., White, R.J., and Sauer, J. (2019). Hydrothermal base catalyzed depolymerization and conversion of technical lignin – an introductory review. Carbon Resour. Convers. 2: 59–71.

Parthasarathi, R., Romero, R.A., Redondo, A., and Gnanakaran, S. (2011). Theoretical study of the remarkably diverse linkages in lignin. J. Phys. Chem. Lett. 2: 2660–2666.

Ragauskas, A.J., Williams, C.K., Davison, B.H., Britovsek, G., Cairney, J., Eckert, C.A., Frederick, W.J., Hallett, J.P., Leak, D.J., Liotta, C.L., et al. (2006). The path forward for biofuels and biomaterials. Science 311: 484–489.

Roberts, V.M., Stein, V., Reiner, T., Lemonidou, A., Li, X., and Lercher, J.A. (2011). Towards quantitative catalytic lignin depolymerization. Chem. Eur J. 17: 5939–5948.

Rößiger, B., Röver, R., Unkelbach, G., and Pufky-Heinrich, D. (2017). Production of bio-phenols for industrial application: scale-up of the base-catalyzed depolymerization of lignin. Green Sustain. Chem. 7: 193–202.

Saisu, M., Sato, T., Watanabe, M., Adschiri, T., and Arai, K. (2003). Conversion of lignin with supercritical water-phenol mixtures. Energy Fuels 17: 922–928.

Schutyser, W., Renders, T., Van Den Bosch, S., Koelewijn, S.F., Beckham, G.T., and Sels, B.F. (2018). Chemicals from lignin: an interplay of lignocellulose fractionation, depolymerisation, and upgrading. Chem. Soc. Rev. 47: 852–908.

Serrano, L., Antonio, J., Cristina, C., and Sancho, G. (2019). Lignin depolymerization to BTXs. Top. Curr. Chem. 377: 26.

Shuai, L., Talebi Amiri, M., and Luterbacher, J.S. (2016). The influence of interunit carbon–carbon linkages during lignin upgrading. Curr. Opin. Green Sustain. Chem. 2: 59–63.

Sulaeva, I., Zinovyev, G., Plankeele, J.M., Sumerskii, I., Rosenau, T., and Potthast, A. (2017). Fast track to molar-mass distributions of technical lignins. ChemSusChem 10: 629–635.

Vigneault, A., Johnson, D.K., and Chornet, E. (2006). Advance in the thermal depolymerisation of lignin via base-catalysis. In: Bridgwater, A.V. and Boocock, D.G. (Eds.), *International conference in science in thermal and chemical biomass. Conversion (STCBC), 30 August–2 September 2004, Victoria, B.C., Canada*. National Renewable Energy Lab. (NREL), Golden, CO (United States), pp. 1401–1419.

Ye, Y., Zhang, Y., Fan, J., and Chang, J. (2012). Novel method for production of phenolics by combining lignin extraction with lignin depolymerization in aqueous ethanol. Ind. Eng. Chem. Res. 51: 103–110.

Yong, T.L.K. and Matsumura, Y. (2012). Reaction kinetics of the lignin conversion in supercritical water. Ind. Eng. Chem. Res. 51: 11975–11988.

Yong, T.L.K. and Matsumura, Y. (2013). Kinetic analysis of lignin hydrothermal conversion in sub- and supercritical water. Ind. Eng. Chem. Res. 52: 5626–5639.

Zakzeski, J., Bruijnincx, P.C.A., Jongerius, A.L., and Weckhuysen, B.M. (2010). The catalytic valorization of lignin for the production of renewable chemicals. Chem. Rev. 110: 3552–3599.

Zhang, B., Huang, H.J., and Ramaswamy, S. (2008). Reaction kinetics of the hydrothermal treatment of lignin. Appl. Biochem. Biotechnol. 147: 119–131.

Zinovyev, G., Sulaeva, I., Podzimek, S., Rössner, D., Kilpeläinen, I., Sumerskii, I., Rosenau, T., and Potthast, A. (2018). Getting closer to absolute molar masses of technical lignins. ChemSusChem 11: 3259–3268.

Supplementary Material: The online version of this article offers supplementary material (https://doi.org/10.1515/hf-2021-0121).